diffraction peaks, respectively, applying the direct comparison method.[37] The following expression has been calculated for determining the fraction x_α of the α-Si_3N_4 phase:

$$x_\alpha = \frac{1}{1 + 0.688\left(\frac{I_\beta}{I_\alpha}\right)} \quad (9)$$

The SEM pictures were recorded with a Philips XL30 microscope at 30 KV from samples ultrasonically dispersed in ethanol, supported on a metallic grill and covered with a thin graphite film.

Final version: February 01, 2002

[1] K. J. Jack, *J. Mater. Sci.* **1979**, *11*, *1135.*
[2] N. H. Cother, P. Hodgson, *Trans. J. Br. Ceram. Soc.* **1982**, *81*, 141.
[3] M. Taguchi, *Adv. Ceram. Mater.* **1987**, *81*, 754.
[4] H. Gleiter, *Prog. Mater. Sci.* **1989**, *33*, 223.
[5] F. K. Van Dijen, U. Vogy, *J. Eur. Cer. Soc.* **1992**, *10*, 273.
[6] M. Ekelund, B. Forslund, *J. Am. Ceram. Soc.* **1992**, *75*, 532.
[7] M. Barsoum, P. Kangatkar, M. J. Koczak, *J.Am. Ceram. Soc.* **1991**, *74*, 1248.
[8] R. G. Pigeon, A. Varma and A. E. Miller, *J. Mater. Sci.* **1993**, *28*, 1919.
[9] H. Lange, G. Wötting, G. Winter, *Angew. Chem. Int. Ed. Engl.* **1991**, *30*, 1579.
[10] A. J. Moulson, *J. Mater. Sci.*, **1979**, *14*, 1071.
[11] G. Ziegler, J. Heinrich, G. Wötting, *J. Mater. Sci.* **1987**, *22*, 3041.
[12] G. Ziegenbalg, T. Focke, H. Holldorf, R. Brink and H. Lange, *J. Mater. Sci.* **1999**, *34*, 2199.
[13] D. L. Segal, *Br. Ceram. Trans. J.* **1986**, *85*, 184.
[14] T. Hashishin, Y. Kaneko, H. Iwanaga, Y. Yamamoto, *J. Mater. Sci.* **1999**, *34*, 2193.
[15] A. W. Weimer, G. A. Eisman, D. W. Susnitzky, D. R. Beaman and J. W. McCoy, *J. Am. Ceram. Soc.* **1997**, *80*, 2853.
[16] M. Komeya, H. Inoue, *J. Mater. Sci. Lett.*, **1975**, *10*, 1243.
[17] S. A. Siddiqi, A. Hendry, *J. Mater. Sci.* **1985**, *20*, 3230.
[18] S. J. P. Durham, K. Shanker, R. A. L. Drew, *J. Am. Ceram. Soc.* **1991**, *74*, 31–37.
[19] S. B. Hanna, N. A L. Mansour, A. S. Taha, H. M. A. Abd-Allah, *Br. Ceram. Trans. J.* **1985**, *84*, 18–21.
[20] A. Rahman, F. L. Riley, *J. Eur. Cer. Soc.*, **1989**, *5*, 11.
[21] H. Yoshimatsu, H. Kawasaki, Y. Miura, A. Osaka, *J. Mater. Sci.*, **1989**, *24*, 3280.
[22] A. S. Sanyal, J. Mukerji, S. Bandyopadhyay, *J. Am. Ceram. Soc.* **1991**, *74*, 2312.
[23] D. Hardie, K. H. Jack, *Nature*, **1957**, *180*, 332.
[24] S. N. Ruddlesden, P. Popper, *Acta Cryst.* **1958**, *11*, 465.
[25] S. Wild, P. Grieveson, K. H. Jack, in *Special ceramic 5* (Ed.: P.Popper), British Ceramic Research Association, Stoke-on-Trent, **1972**, pp. 385–395.
[26] M. Mitomo, in *Silicon Nitride-1* (Eds.: S. Somiya, M. Mitomo, M. Yashima), Elsevier Applied Science, London **1990**, pp. 1–11
[27] J. A. Wendel, W. A. Goddard III, *Chem. Phys.*, **1992**, *97*, 5048.
[28] I. Higgings, A. Hendru, *Br. Ceram. Trans. J.* **1986**, *85*, 161.
[29] E. Kormeijer, C. Scholte, E. Blömer, R. Metoelaan, *J. Mater. Sci.* **1990**, *25*, 1261.
[30] L. A. Pérez-Maqueda, J. M.Criado, J. Subrt, C. Real, *Catalysis Letters*, **1999**, *60*, 151.
[31] L. A. Pérez-Maqueda, J. M.Criado, C. Real, J. Subrt, J. Bohacek, *J. Mater. Chem.*, **1999**, *9*, 1839.
[32] G. S. Chopra, C. Real, M. D. Alcala, L. A. Perez-Maqueda, J. Subrt, J. M. Criado, *Chem. Mater.* **1999**, *11*, 1128.
[33] T.Hatakeyama, Z.Liu (Eds.), *Handbook of thermal analysis*, J. Wiley & Sons, New York *1998*, Chap. 3.
[34] S. Shimada, T. Kataoka, *J. Am. Ceram. Soc.* **2001**, *84*, 2442.
[35] M. V. Vlasova, T. S. Barnitskaya, L. L. Sukhikh, L. A. Krusninkaya, T. V. Tomila, S. Yu Artyuch, *J. Mater. Sci.* **1995**, *30*, 5263.
[36] A. W. Weimer, G. A. Eisman, D. W. Susnitzky, D. R. Beaman, J. W. McCoy, *J. Am. Ceram. Soc.* **1997**, *80*, 2853.
[37] B. D. Cullity, *Elements of X-ray diffraction*, Adisson-Wesley Publ. Co., London **1978**, p. 397.

Novel Synthesis of Orthopaedic Implant Materials**

By *Arvind Varma*,* *Bingyun Li*, and *Alexander Mukasyan*

About 400,000 hip and knee joints are replaced annually using artificial implants in the United States alone.[1] The ability of orthopaedic implants to provide rapid healing and long-term clinical performance has been proven over many decades to offer patients a high quality of life while minimizing health care costs. In general, cobalt and titanium based alloys, as well as stainless steels, are the major metallic materials used for orthopaedic products. Among these, cobalt-chromium-molybdenum (CoCrMo) alloys demonstrate perhaps the most useful balance of resistance to corrosion, fatigue and wear, along with strength and biocompatibility.[2]

[*] *Prof. A. Varma, Dr. B. Li, Prof. A. Mukasyan*
Department of Chemical Engineering and Center for Molecularly Engineered Materials
University of Notre Dame, Notre Dame, IN 46556 (USA)
E-mail: avarma@nd.edu

[**] *The financial support by the 21st Century Research & Technology Fund, State of Indiana, is gratefully acknowledged. We also thank Dr. Ravi Shetty, Zimmer, Inc., Warsaw, IN, USA for his interest in this work and assistance with materials characterization.*

  1438-1656/02/0707-0482 $ 17.50+.50/0

CoCrMo alloys are used in a wide range of orthopaedic implants, such as total hip and knee replacements, as well as bone screws, plates, and wires.[3,4] Moreover, a large fraction of dental devices and some cardiovascular prostheses, mainly heart valves, are produced from these materials. Currently, these widely used CoCrMo alloys are produced by conventional furnace technology. Owing to high melting points of the main alloy elements (e.g., $T_{mp,Co}$ ~ 1,768 K), high-temperature furnaces and long process times (several hours) are required. Further, alloys produced by conventional methods may contain microstructural inhomogeneities such as carbide segregation (e.g., networking and pooling), which make the materials difficult to hot work and may cause implant fracture.[5] Even inside the human body, implants may produce wear debris, which causes osteolytic loosening.[6] For this reason, a major concern of implant research is to improve the hardness related wear resistance of artificial components. Therefore, all attempts to develop more efficient and flexible methods for production of such alloys with superior properties are of great interest.

The synthesis of materials using combustion phenomena is an advanced approach in powder metallurgy.[7] The process is characterized by unique conditions involving extremely fast heating rates (up to 10^6 K/s), high temperatures (up to 3,500 K), and short reaction times (on order of seconds).[8,9] As a result, combustion methods offer several attractive advantages over conventional metallurgical processing and alloy development technologies. The foremost is that solely the heat of chemical reaction (instead of an external source) supplies the energy for the synthesis. Also, simple equipment, rather than energy-intensive high-temperature furnaces, is sufficient. Further, an attractive aspect of combustion process is its ability to produce materials of high-purity, since the high temperatures purge the powders of any volatile impurities adsorbed or present in the reactants. Remarkably, the high temperature gradients, combined with rapid cooling rates in the combustion wave, may form metastable phases and unique microstructures not possible by conventional methods. In addition, this technique allows the synthesis of new alloy compositions conveniently, rapidly, and in relatively small amounts that permit rapid screening of material composition to enhance properties. Finally, the combustion method also permits scale-up, so that commercial quantities can be produced efficiently.

A critical problem to produce structural engineering parts by combustion process is that the resulting parts are typically porous.[10,11] Thus various methods, including extrusion and shock-wave loading, are utilized to densify the porous products.[12,13] However, these methods incur economic penalty, and application of high pressure during combustion tends to prevent purification of the product. In the present work, we report a novel approach, i.e. the use of low pressure, to achieve fully dense materials with high purity. This *low-pressure combustion synthesis (LPCS)* allows one to obtain pore-free CoCrMo orthopaedic implants without applied force in a single step. Using the rapid screening ability of this technique, we have synthesized novel materials with unique microstructures and enhanced properties.

To produce CoCrMo alloy, a thermite type Co_3O_4-Co-Cr-Mo-Al system was selected. The following reaction occurs in the combustion wave front:

$$3Co_3O_4 + 8Al + (x\text{Co}, y\text{Cr}, z\text{Mo}) \longrightarrow 4Al_2O_3 + 9\text{Co-based alloy} \quad (1)$$

where Al is the reducing agent, and x, y and z coefficients can be varied to obtain the desired compositions and combustion temperatures.

Thermodynamic analysis[14] shows that the adiabatic combustion temperature (T_{ad}) for the above reaction at 1 atm Argon ambient atmosphere can be as high as 2,900 K (Fig. 1). By increasing pure Co content in the initial mixture (i.e. the value of x), T_{ad} decreases continuously, while the amount of gaseous products (including Cr, Co, Al, oxides, etc.) decreases, reaching a minimum at 0.6 mole ratio of Co to (Co+Co_3O_4). Thus to have T_{ad} higher than the melting points of Al_2O_3 (T_{mp,Al_2O_3} ~2,300 K) and Co-based alloy ($T_{mp,alloy}$ ~ 1,768 K), important for full separation and homogeneous composition distribution along with low amount of gas products, 0.5 mole ratio of Co to (Co + Co_3O_4) was selected as the basic reactant composition.

It is found that the phase separation between Al_2O_3 and Co-alloy takes place in the combustion wave due to their density differences and surface tension.[15] However, even for calculated optimum compositions, experiments under normal ambient pressure show that gas released in the high temperature reaction zone leads to the formation of pores and cavities in the final products (Scheme 1, route a→f). Such defects are due to the crystallization of an Al_2O_3 "cap" on top of the melt Co-alloy product at high temperature, which prevents gas escape and leads to undesired porous microstructure (Scheme 1, f).

A unique fundamental aspect of the present work is that low ambient gas pressure allows one to achieve pore-free

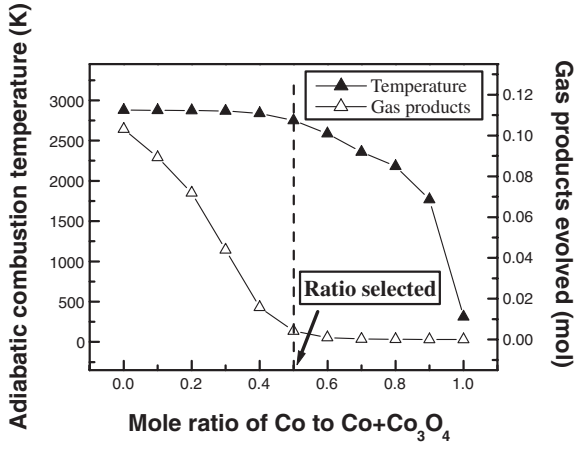

Fig. 1. Dependence of adiabatic combustion temperature and gas product evolution on initial reactant mixture composition; ambient gas pressure: 1 atm Argon.

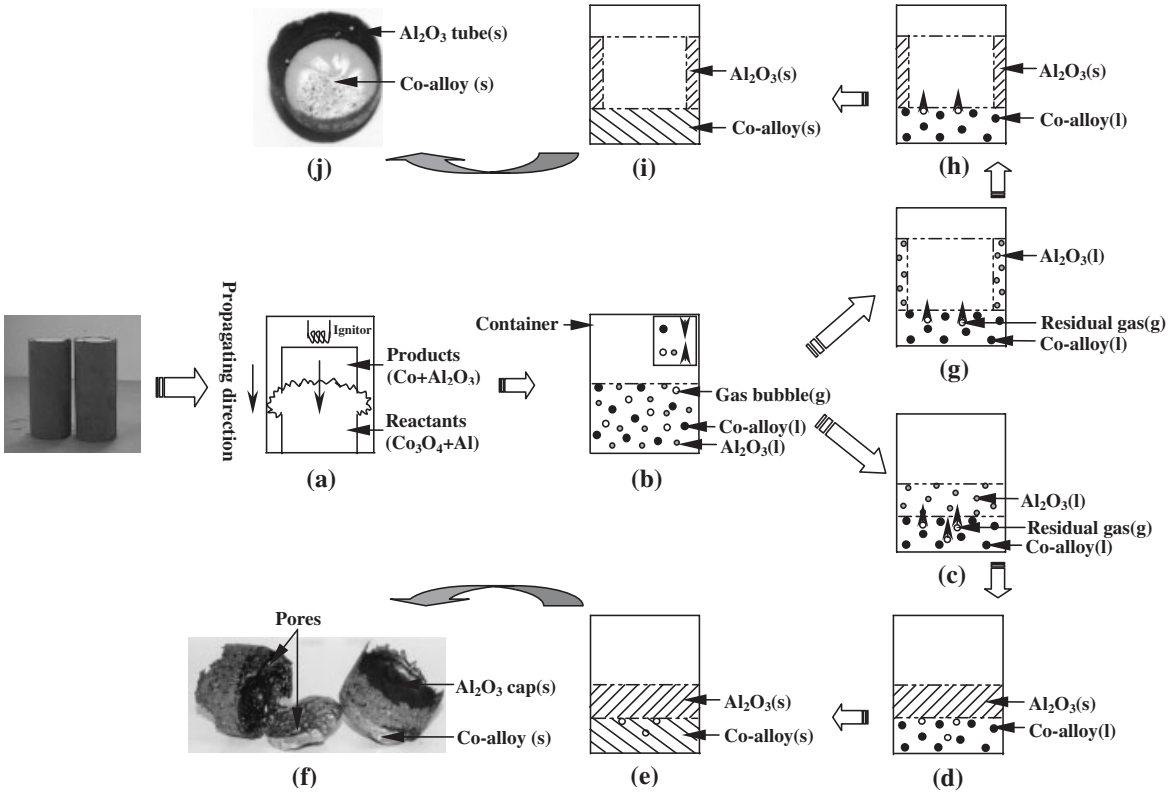

$$Co_3O_4+Al + (Co, Cr, Mo) \Rightarrow \text{Co-alloy} + Al_2O_3$$

Scheme 1. Mechanism for formation of CoCrMo alloys. Route a→f shows that under normal ambient pressure, after phase separation between Al_2O_3 and the Co-based alloy, an undesired Al_2O_3 "cap" appears. Using the proposed LPCS technology (route a-b-g→j), a thin Al_2O_3 tube forms which permits the full release of gas and the synthesis of a pore-free alloy product.

(> 99 % theoretical density) alloy at high yield (> 90 %). The yield is defined here as ratio of the metal product mass to the theoretical metal mass formed from reaction. According to the experimental results shown in Figure 2, at pressures lower than 0.15 atm (region I), a pore-free alloy can be produced but the yield is only 60 % or lower. On the other hand, at pressures exceeding 0.2 atm (region III), the yield is more than 90 % but the material density is too low. Remarkably, it is found that there exists a window of ambient gas pressures (region II) where *both* yield and density simultaneously possess acceptably high values. These experimental results can be explained as follows.

In region III, phase separation occurs following route (a)→(f) in Scheme 1 as described above. In regions I and II, instead of a cap, Al_2O_3 separates from the metal alloy in the form of a thin (~ 1mm) tube coating the internal surface of the container (Scheme 1, route a-b-g→j). The formation of the thin ceramic tube is believed to be related to the gas pressure difference between the ambient atmosphere and inside the product melt, as well as differences in the wettability characteristics of the container wall and product phases. The absence of the alumina cap further speeds up the release of residual gas from the melt alloy bulk, thus leading to a pore-free material and also avoiding problems of alloy-slag adhe-

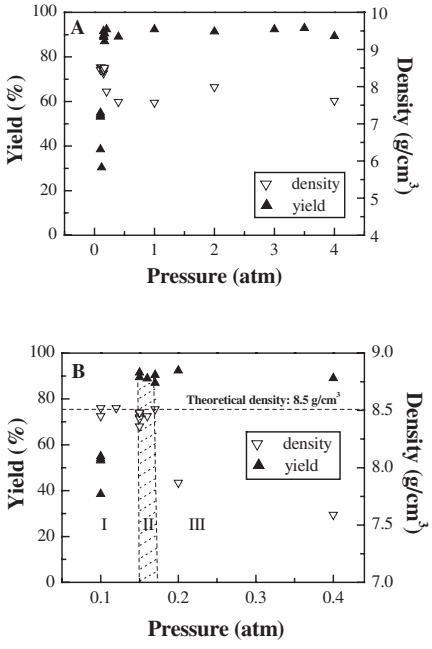

Fig. 2. (a) Influence of ambient gas pressure on alloy density and yield. (b) Enlargement of low pressure region of (a). Region (I) has high density but low yield; region (III) has high yield but low density; region (II) exhibits high density and high yield simultaneously.

ADVANCED ENGINEERING MATERIALS

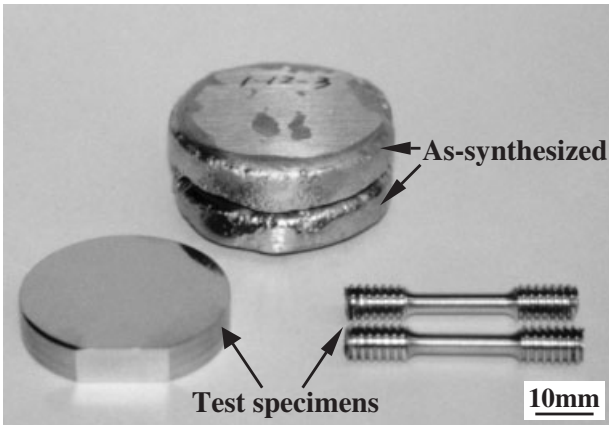

Fig. 3. As-synthesized samples and machined specimens for testing.

sion. However, in region I, yield reduces owing to partial alloy-product blowout, which occurs as a result of the larger pressure gradient existing between the alloy bulk and ambient atmosphere. Thus the desired proper balance between full gas release and high yield is achieved in region II and forms the basis of the proposed LPCS technique.

Figure 3 shows the as-synthesized Co-alloy ingots produced by LPCS, along with machined test specimens. It may be seen that near-net shaped disks with smooth surfaces are produced, and no cavities or pores are observed. Chemical analysis shows that the alloy compositions match well the ASTM F75 standard specifications and exhibit extremely low levels of impurities (Table 1). Note that Ni possesses allergic potential,[16] and Si can cause embrittlement,[17] thus smaller amounts of such elements in product alloy are important.

Along with the combustion synthesis related technological advantages noted earlier, the LPCS method offers the opportunity to synthesize materials with unique microstructures and properties. Using the rapid screening ability of the technique, we investigated a wide range of material compositions. In this context, graphite, carbon black and several carbides (e.g., TiC, Cr_3C_2) were used as additives to synthesize novel materials with superior properties. For example, it is known that carbon enhances mechanical properties in cast CoCrMo alloys,[18] which was also confirmed here using graphite or carbon black as additives (Fig. 4a). We showed next that, among the various additives, Cr_3C_2 is the most effective one for increasing the material hardness (Fig. 4b). The hardness of alloys with different amounts of Cr_3C_2 is shown in Figure 4c. These values are significantly higher than those exhibited by alloys synthesized by conventional techniques, such as the wrought CoCrMo alloys,[19] and are also

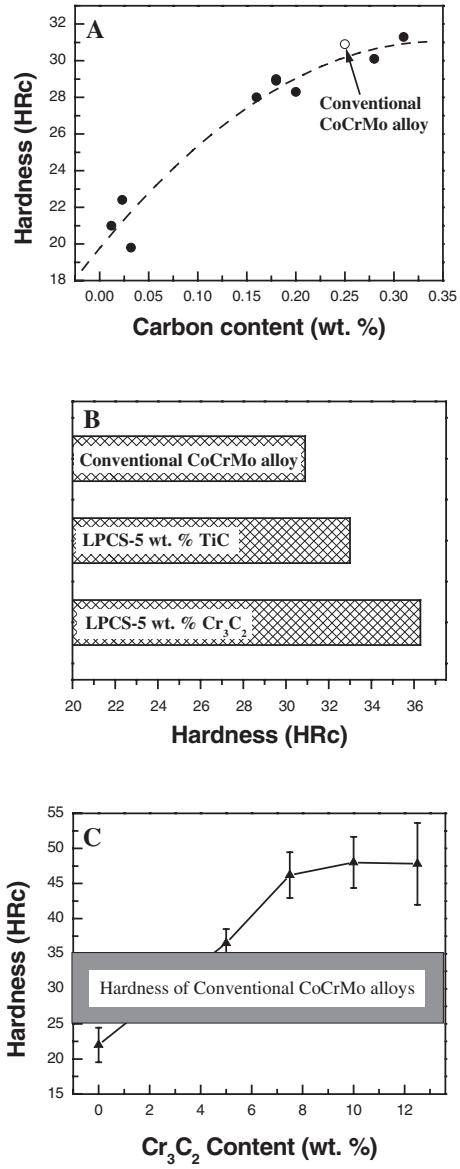

Fig. 4. Influence of different additives on hardness of LPCS-synthesized Co-based alloys. (a) Hardness increases with increasing addition of graphite or carbon black. (b) For the same extent of carbide additives, Cr_3C_2 exhibits the most hardness enhancement. (c) Dependence of alloy hardness on Cr_3C_2 content (bars, standard deviation).

much higher than for the LPCS-alloys produced with addition of graphite or carbon black (Fig. 4a). This enhancement owes to the differences in alloy microstructures, although containing the same amount of carbon, as shown in Figure 5. It may be seen that the microstructure of LPCS-alloy (Fig. 5b) is finer and more uniform as compared to the conventional

Table 1. Chemical composition (wt.-%) of the CoCrMo alloy produced by LPCS and related ASTM standard specifications.

Composition		Co	Cr	Mo	Si	W	Al	Fe	Mn	Ni	P	B	N
F75-98	min	bal	27.0	5.0	...	...	...	...	...	...	...	...	...
	max	bal	30.00	7.00	1.00	0.20	0.30	0.75	1.00	1.00	0.020	0.01	0.25
LPCS-CoCrMo		bal	28.01	6.47	0.076	0.13	0.20	0.11	0.085	0.08	0.009	<0.0005	0.0058

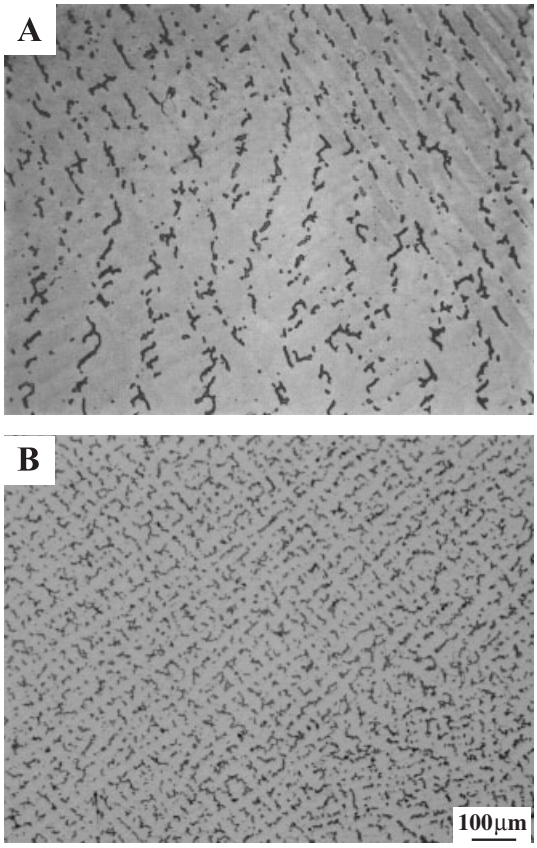

Fig. 5. Typical microstructures of pore-free CoCrMo orthopaedic implant alloys containing 0.33 wt.% C produced by conventional (a) and LPCS (b) methods.

one (Fig. 5a). This effect results from the unique LPCS conditions and its mechanism is as follows.

Carbon has a high melting point (~ 3,800 K) and hence does not melt under conventional synthesis or LPCS conditions, so that it is difficult to distribute the formed carbon containing phases homogeneously. However, metal carbides which have a lower melting point (e.g., T_{mp} for Cr_3C_2 is 2,168 K), can be added directly to the initial reactant mixture. In this case, owing to high temperatures in the combustion wave (~ 2,900 K), these carbides melt and distribute uniformly during LPCS (Fig. 5b), while they remain in the original solid state during the relatively low temperatures (~ 2,000 K) involved in conventional casting techniques. These features permit LPCS-alloys to attain hardness values up to 46 HRc, approximately 50 % higher than conventional alloys with the same carbon content (0.33 wt.-%).

The aforementioned concept of LPCS, i.e. achieving full release of residual gas formed during reaction by adjusting ambient gas pressure to form a ceramic tube, can also be used in other reaction systems to produce pore-free alloys, ceramics, intermetallics and composites. For example, synthesis of dense stainless steel based biomaterials using this technology as follows:

$$Fe_2O_3 + 2Al + (Cr, Mo) \longrightarrow Al_2O_3 + \text{stainless steel alloy} \qquad (2)$$

also shows promise and is currently under investigation.

In summary, a novel method for synthesis of biomedical alloys has been developed based on combustion phenomena. The work focused on the synthesis of Co-based alloys, which cover a wide range of orthopaedic implants, including total hip and knee replacements, as well as bone screws, plates, and wires. The new process successfully combines two important features involving *self-densification* and *self-purification*, which result in production of high-purity pore-free implants of precise chemical and phase compositions in one step without applied force, and shows great commercial potential for different applications. Using the rapid screening ability of this technique, new alloys with superior properties, which are expected to produce innovative orthopaedic implants, have also been developed.

Received: January 04, 2002
Final version: March 25, 2002

[1] *Orthopaedic Network News* **2000**, *11*, 3.
[2] D. Granchi, G. Ciapetti, S. Stea, L. Savarino, F. Filippini, A. Sudanese, G. Zinghi, L. Montanaro, *Biomater.* **1999**, *20*, 1079.
[3] D. F. Williams, in *Biocompatibility of Clinical Implant Materials* (Ed. D. F. Williams), CRC Press, Inc., Boca Raton, Florida **1981**, p. 99.
[4] S. K. Yen, S. W. Hsu, *J. Biomed. Mater. Res.* **2001**, *54*, 412.
[5] M. Gómez, H. Mancha, A. Salinas, J. L. Rodríguez, J. Escobedo, M. Castro, M. Méndez, *J. Biomed. Mater. Res.* **1997**, *34*, 157.
[6] R. Varano, S. Yue, D. Bobyn, J. B. Medley, in *Alternative Bearing Surfaces in Total Joint Replacement* (Eds. J. J. Jacobs, T. L. Craig), ASTM Committee, San Diego, Calif., Nov. 11-12, **1997**, ASTM STP 1346, **1998**, p. 55.
[7] A. Varma, A. S. Mukasyan, in *Powder Metal Technologies and Applications*, ASM Handbook, *7*, ASM International, Materials Park, Ohio, **1998**, p. 523.
[8] A. G. Merzhanov, in *Combustion and Plasma Synthesis of High-temperature Materials* (Eds: Z. A. Munir, J. B. Holt), VCH Publishers, New York, **1990**, p. 1.
[9] A. Varma, *Sci. Am.* **2000**, *283 (8)*, 58.
[10] S. D. Dunmead, Z. A. Munir, J. B. Holt, D. D. Kingman, *J. Mater. Sci.* **1991**, *26*, 2410.
[11] A. Varma, A. S. Rogachev, A. S. Mukasyan, S. Hwang, *Advances in Chem. Eng.* **1998**, *24*, 79.
[12] V. V. Podlesov, *J. Eng. Phys. Thermophys.* **1992**, *63*, 1065.
[13] J. Lee, N. N. Thadhani, H. A. Grebe, *Metall. Mater. Trans.* **1996**, *27A*, 1749.
[14] A. A. Shiryaev, *Int. J. SHS* **1995**, *4*, 351.
[15] A. Mukasyan, A. Pelekh, A. Varma, A. Rogachev, A. Jenkins, *AIAA J.* **1997**, *35*, 1821.
[16] J. C. Wataha, P. E. Lockwood, M. Marek, M. Ghazi, *J. Biomed. Mater. Res.* **1999**, *45*, 251.
[17] A. V. Nikolaeva, Y. A. Nikolaev, Y. R. Kevorkyan, A. M. Kryukov, Y. N. Korolev, *Atomoc Energy* **2000**, *88*, 281.

[18] R. Tandon, in *Cobalt-Base Alloys for Biomedical Applications* (Eds. J. A. Disegi, R. L. Kennedy, R. Pilliar), ASTM Committee, Norfolk, Virginia, Nov. 3–4, **1998**, ASTM STP 1365, **1999**, p. 3.
[19] R. H. Shetty, in *Encyclopedic Handbook of Biomaterials and Bioengineering* (Ed. D. L. Wise), Marcel Dekker, New York **1995**, part B 1, p. 509.

Preparation of Al_2O_3, TiO_2, and Hydroxyapatite Ceramics with Pores Similar to a Honeycomb Structure

By *Rosemarie Dittrich*, *Gerhard Tomandl*,* and *Martina Mangler*

Alginate gelation is one of few methods that can produce porous ceramics with oriented tubular pores. Alginates are well known as inorganic polymers that can be gelled by cross-linking with multivalent metal ions. This process allows the production of structured alumina, titania, and hydroxyapatite ceramics with an approximately honeycomb structure.

The primary thin layer has the function of a selective membrane through which the slurry gradually transforms into the gel.

The gel-like substance was dried by various methods such as air drying, supercritical drying, and freeze drying. The main problem is very high shrinkage occurring during the transition from the wet gel to the sintered body. The samples were fired at various temperatures and had a high porosity of up to 80 %. The bulk density, tensile splitting strength, and a narrow pore and capillary size distribution were measured. The ceramics have a bimodal pore size distribution when measured by mercury porosimetry. The first peak represents the pores between the capillaries, the second is caused by the capillaries themselves. The pores between the capillaries almost disappear with increasing sintering temperature.

The spatial pore structure was investigated by serial sectioning and image analysis. An increase in pore size and homogenization of pore arrangement led to the formation of capillaries.

This process offers new possibilities for preparing porous ceramics with uniform parallel capillaries, which might be useful as membranes, catalyst supports, gas or chemical sensors, or for implants.

[*] *R. Dittrich, Prof. G. Tomandl, M. Mangler*
Institut für Keramische Werkstoffe, TU Bergakademie Freiberg
Gustav-Zeuner-Str. 3, D-09596 Freiberg (Germany)
E-mail: tomandl@ikw.tu-freiberg.de

The starting powder was dispersed in aqueous solution at pH 6 with Na alginate to give a slurry. It is important to control the pH to produce stable slurries. Na alginate slurry is stable at pH 5–10. The average particle sizes of the powders are shown in Table 1 (Microtrac Ultrafine Particle Analyzer; Leeds & Northrup). The isoelectric points of the materials are also given in Table 1.

Then a solution of divalent metal ions (Me^{2+}) are deposited onto the surface of the slurry.

The slurry can be gelled by ion exchange of Na^+ in the alginate with divalent metal ions such as Cu^{2+}, Cd^{2+}, Pb^{2+}, Ca^{2+}, Zn^{2+}, and Sr^{2+}. The gelation reaction is

$$2\ \text{Na alginate (aq.)} + Me^{2+} \rightarrow \text{Me alginate}_2 + 2\ Na^+ \quad (1)$$

Immediately a primary thin gel layer is formed. The primary gel layer has the function of a selective membrane, allowing the passage of the metal ions (Me^{2+}) but not other ions (such as ions of Na alginate and Al_2O_3). Owing to diffusional control of Me^{2+} transport through the membrane, the slurry gradually transforms to the gel resulting in the formation of capillaries in the direction of Me^{2+} diffusion. The metal ions and also the anions have an effect on the size of the capillaries.[1] The concentration of electrolyte also influenced the capillaries: the higher the concentration the smaller and fewer the capillaries.

After gelation, the primary membrane and the gel bottom are cut away. To remove Me^{2+} impurities, ion exchange is carried out.[2–4] Figure 1 shows the preparation process illustrated with scanning electron microscopy (SEM) images of Al_2O_3 samples.

The samples made have a diameter of approximately 5–10 mm and a length of 3–6 mm, a high porosity up to 90 %, and a capillary diameter of 10–30 μm, depending on the ceramic material and process conditions.

For the production of structured ceramics stable ceramic slurries are necessary. At pH 6 these powders can be structured. Lower pH leads to alginate threads in the slurry, and no structuring is possible.

The structuring process is determined by the diffusion of the metal ions through the primary membrane into the sol. The depth of diffusion was measured against time. After 48 h a gel thickness of 30 mm was achieved.

The gels were examined by stereomicroscopy, and dried and sintered samples were viewed by SEM.

Table 1. Particle sizes and isoelectric points of powders.

Material	Particle size (d_{50}) [μm]	Isoelectric point
Al_2O_3 (Alcoa A16)	0.35	8.4
Hydroxyapatite (Merck)	4.30	7.8
TiO_2 (Degussa)	0.19	6.3

  1438-1656/02/0707-0487 $ 17.50+.50/0